PREDICTION OF SALT CAVERN DIAMETERS AND DEPTH FROM SUBSIDENCE DATA

S. Archeeploha & K. Fuenkajorn

Geomechanics Research Unit, Institute of Engineering,
Suranaree University of Technology, Muang District,
Nakhon Ratchasima, Thailand 30000.
Phone (66-44) 224-758, Fax (66-44) 224-448
E-Mail: kittitep@sut.ac.th

Keyword: Subsidence, brine, cavern, sinkhole

ABSTRACT: An analytical method has been developed to predict the location, depth and size of caverns created at the interface between salt and overlying formations. A governing hyperbolic equation is used in a statistical analysis of the ground survey data to determine the cavern location, maximum subsidence, maximum surface slope and surface curvature under the sub-critical and critical conditions. The regression produces a set of subsidence components and a representative profile of the surface subsidence under sub-critical and critical conditions. Finite difference analyses using FLAC code correlate the subsidence components with the cavern size and depth under a variety of strengths and deformation moduli of the overburden. A set of empirical equations correlates these subsidence components with the cavern configurations and overburden properties. For the super-critical condition, a discrete element method (using UDEC code) is used to demonstrate the uncertainties of the ground movement and sinkhole development resulting from the complexity of the post-failure deformation and joint movements in the overburden.

1 INTRODUCTION

Salt and associated minerals in the Khorat and Sakon Nakhon basins, northeast of Thailand have become important resources for mineral exploitation and for use as host rock for product storage. For over four decades, local people have extracted the salt by using an old fashioned technique, called here the 'brine-pumping' method. A shallow borehole is drilled into the rock unit directly above the salt. Brine (saline groundwater) is pumped through the borehole and left to evaporate on the ground surface. Relatively pure halite with slight amounts of associated soluble minerals is then obtained. This simple and low-cost method can however cause an environmental impact in the form of unpredictable ground subsidence, sinkholes and surface contamination (Fuenkajorn, 2002). Even though the brine pumping industry has been limited to strictly controlled areas, isolated from agricultural areas and farmlands, severe surface subsidence and sinkholes have commonly been found outside the controlled areas, particularly on the upstream side of the groundwater flow (Figure 1).

The subsidence is caused by deformation or collapse of the cavern roof at the interface between the salt and overburden. Precise locations of the dissolved caverns are difficult to determine due to the complexity of groundwater circulation, infiltration of fresh surface water,

brine pumping rates, and number and intensity of the pumping wells.

As a result, location and magnitude of the subsidence are very unpredictable. Exploratory drilling and geophysical methods (e.g., resistivity and seismic surveys) have normally been employed to determine the size, depth and location of the underground cavities in the problem areas in an attempt to backfill the underground voids, and hence minimizing the damage of the engineering structures and farmland on the surface (Jenkunawat, 2005, 2007; Wannakao, 2004, 2005). The geophysical and drilling investigations for such a widespread area are costly and time-consuming. This calls for a quick and low cost method to determine the size, depth and location of the solution caverns. The method should be used as an early warning tool so that mitigation can be implemented before the uncontrollable and severe subsiding of the ground surface occurs.

The objective of this research is to develop a method to predict the location, depth and size of solution caverns created at the interface between the salt and the overlying formation. The effort includes statistical analysis of the ground survey data in the subsiding areas, numerical simulations to correlate subsidence components with the overburden properties, cavern diameter and depth, and formulation of empirical relations between the cavern configurations and the subsidence components.

2 SITE CONDITIONS

Rock salt in the Maha Sarakham formation, northeast of Thailand is separated into two basins: the Sakon Nakhon basin and the Khorat basin. Both basins contain three distinct salt units: Upper, Middle and Lower members. Figure 2 shows a typical stratigraphic section of the Maha Sarakham formation. The Sakon Nakhon basin in the north covers an area of approximately 17,000 square kilometers. The Khorat basin in the south covers more than 30,000 square kilometers (Figure 3). Warren (1999) gives a detailed description of the salt and geology of the basins. From over 300 exploratory boreholes drilled primarily for mineral exploration, Suwanich (1978) estimates the geologic reserve of the three salt members from both basins as 18 MM tons. Vattanasak (2006) has re-compiled the borehole data and proposes a preliminary design for salt solution mining caverns based on a series of finite element analyses, and suggests that the inferred reserve for solution mining of the Lower Salt member of the Khorat basin is about 20 billion tons. This estimate excludes residential and national forest areas. Figure 3 also shows the areas where the brine pumping has been practiced. Depths of the shallowest salt in those areas vary from 40 m to 200 m. It belongs to the Middle or Lower member, depending on locations. Most of the brine pumping practices are however in the areas where the topography is flat, groundwater table is near the surface, and the salt depth is less than 50 m in the Sakon Nakhon basin, and about 100 m in the Khorat basin (Jenkunawat, 2005; Wannakao, 2005). The overburden consists mainly of mudstone siltstone and sandstone of the Middle Clastic, and claystone and mudstone of the Lower Clastic, with fractures typically dipping less than 30 degrees, and rarely at 70 degrees (Crosby, 2007). The members are characterized by abundant halite and anhydrite-filled fractures and bands with typical thickness of 2 cm to 5 cm.

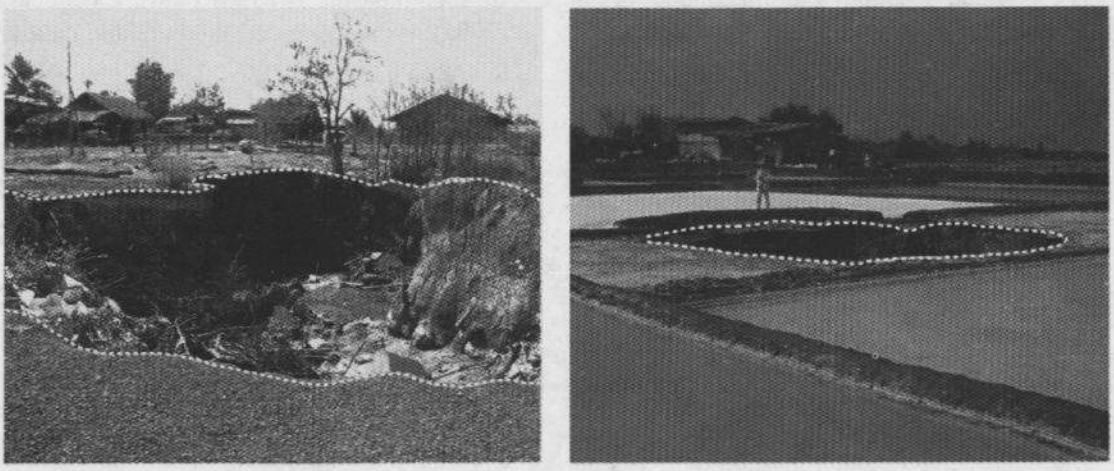

Figure 1. Some sinkholes caused by brine pumping at Nonsabaeng village, Nongkwang, Banmuang district, Sakon Nakhon. (***From Wannakao et al.***, 2004).

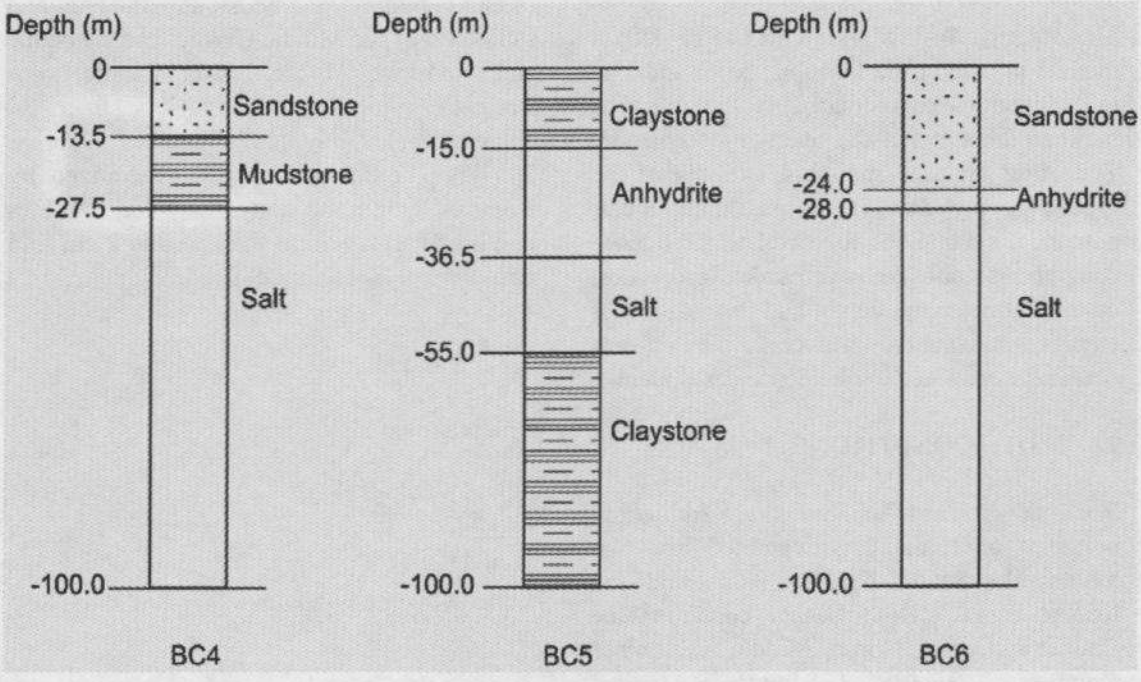

Figure 2. Stratigraphic units from some boreholes **near brine pumping areas in the Sakon Nakhon basin** (modified from Jenkunawat, 2005).

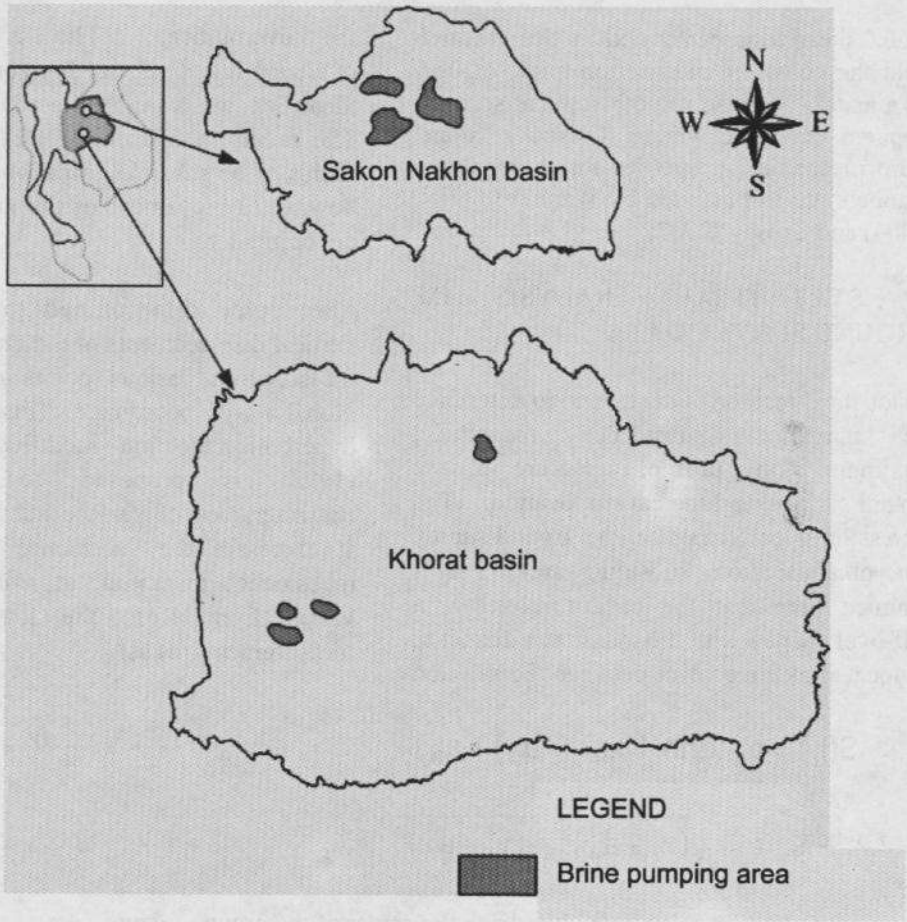

Figure 3. Brine pumping areas in Khorat and Sakon Nakhon salt basins.

Direct shear tests performed in this research yield the cohesion and friction angle of 0.30 MPa and 27° for the smooth saw-cut surfaces prepared from the Middle Clastic siltstone. More mechanical properties for these clastic members are summarized by Wannakao et al. (2004) and Crosby (2007).

3 STATISTICAL ANALYSIS OF GROUND SURVEY DATA

A statistical method is developed to determine the maximum subsidence magnitude, maximum slope profile, curvature of the ground surface, and the cavern location. The regression is performed on the ground survey data obtained from subsiding areas. It is assumed here that the cavern model is a half-oval shaped with the maximum diameter, w, located at the contact between the salt and the overburden. The ground surface, overburden and salt are horizontal. Figure 4 identifies the variables used in this study. The radius of influence (B/2) represents the radius of he subsiding area where the vertical downward movement of the ground equals 1 cm or greater.

The survey data referred to here are the vertical displacements of the ground surface (z) measured at various points respected to a global x-y coordinate (Figure 5). A hyperbolic function modified from Singh (1992) is proposed to govern the characteristics of surface subsidence profile. It expresses the subsidence function, $S(r_i)$ (subsidence magnitude at point 'i', where i varied from 1 to the total number of measurements, n) as:

$$S(r_i) = a_0 \tanh(10a_1 r_i - a_2) + a_3 \qquad (i = 1, 2, 3, \ldots, n) \qquad (1)$$

where $$r_i = \sqrt{(x_i - a_4)^2 + (y_i - a_5)^2} \qquad (2)$$

r_i = distance from data point 'i' to the center of the group of data,
x_i, y_i = coordinates of subsidence measured at point 'i'
a_0, a_1, a_2, a_3, a_4 and a_5 are constants related to the subsidence components and coordinates of the maximum subsidence location, which can be defined as:
a_0 = half of the maximum subsidence (S_{max}),
a_1 = scaling factor,
a_2 = planar offset,
a_3 = vertical offset,
$a_4 = \Sigma x_i/n$, and
$a_5 = \Sigma y_i/n$.

Similarly the maximum slope (G) of the surface subsidence induced at the inflection point can be determined as:

$$G = S'(r_i) = 10a_0 \times a_1 \operatorname{sech}^2(10a_1 r_i - a_2) \qquad (3)$$

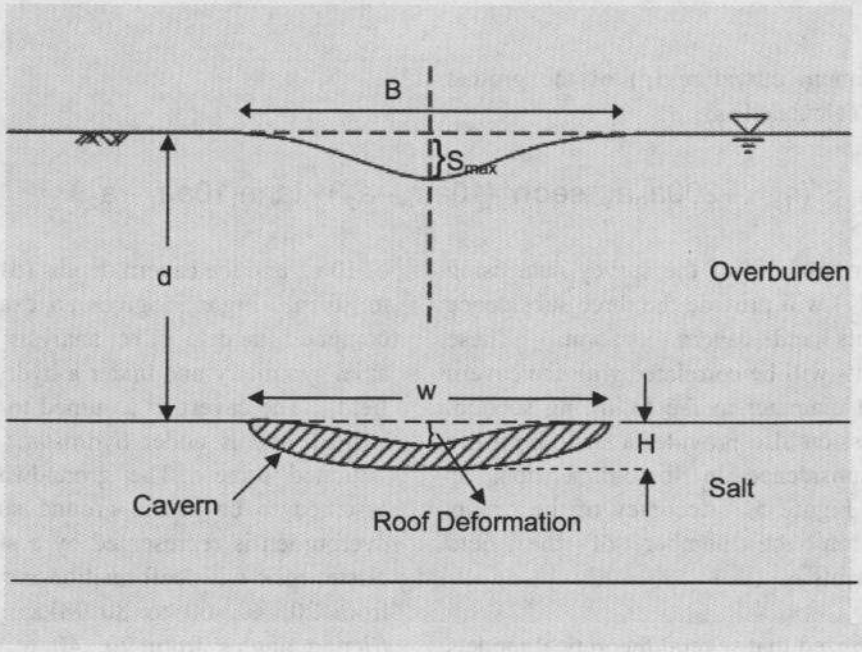

Figure 4. Variables used in this study.

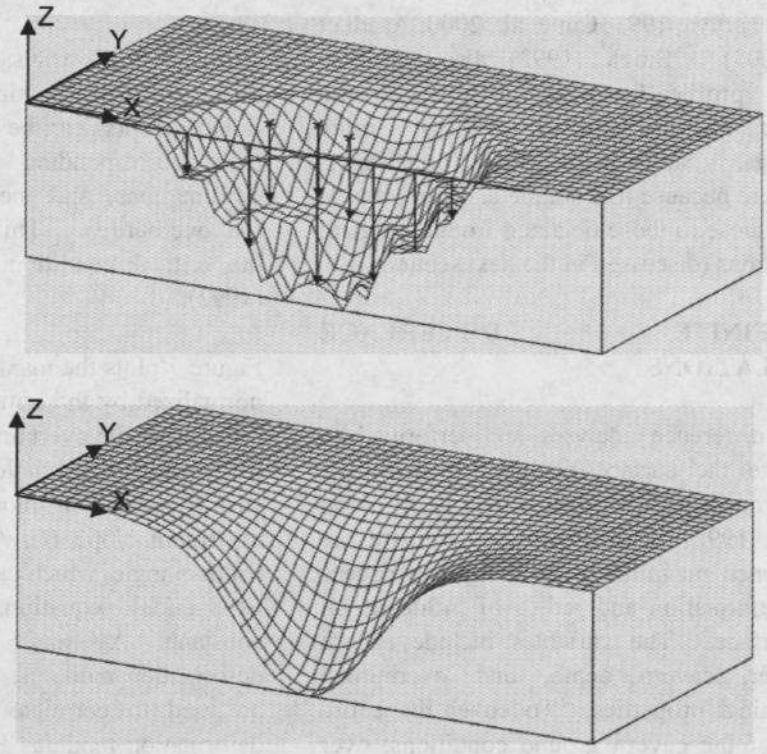

Figure 5. Regression of ground survey data (top) to obtain a representative hyperbolic profile of ground surface (bottom). Vertical scale is greatly exaggerated.

The maximum curvature (ρ) of the ground surface is calculated as:

$$\rho = S''(r_i) = -200a_0a_1^2 \operatorname{sech}^2(10a_1r_i - a_2) \times \tanh(10a_1r_i - a_2) \quad (4)$$

Regression analysis of the survey data using equation (1) will provide the three subsidence components and cavern location. These components will be correlated with the cavern depth and diameter in the following section. The regression also provides a smooth profile of the subsidence in three-dimension, as shown in Figure 5. Accuracy of the results depends on the number of the field measurements.

It is recognized that several theoretical models and governing equations have been developed to predict the subsiding characteristics of the ground surface induced by underground openings (e.g., Nieland, 1991; Shu and Bhattacharyya, 1993; Cui et al., 2000; Asadi et al., 2005). Singh (1992) also proposes several profile functions to represent the subsidence characteristics above mine openings. Singh's hyperbolic function is used here because it is simple and can provide results close to those obtained from numerical simulations (discussed in the next section).

4 FINITE DIFFERENCE SIMULATIONS

Finite difference analyses are performed to correlate the surface components with the cavern depth and diameter. The FLAC code (Itasca, 1992) is used here to simulate the subsidence magnitude, surface slope, cavern roof deformation and radius of influence on the surface. The variables include cavern diameter, cavern depth, and overburden mechanical properties. To cover the entire range of the cavern ground conditions, over 400 finite difference meshes have been constructed to represent cavern diameters (w) varying from 20 m to 100 m with an interval of 10 m, and the cavern depths (d) from 40, 60 to 80 m. Figure 6 gives an example of the computer model. The analysis is made in axial symmetry and under a hydrostatic stress field. The cavern is assumed to be half-oval shaped, and is under hydrostatic pressure of saturated brine. The groundwater table is assumed to be at the ground surface. The overburden is represented by a single unit of clastic rock with deformation moduli varying from 20, 40, 60 to 80 MPa, and internal friction angles from 20, 40 to 60 degrees. The cohesion equals zero in all cases. The mechanical properties of the clastic rock used here are within the range of those compiled by Thiel and Zabuski (1993).

After several trials, the critical cavern diameters (the maximum diameter before failure occurs) can be determined along with their corresponding cavern depths, roof deformations, and mechanical properties of the overburden. This, therefore represents the critical condition as defined by Singh (1992).

Figure 7 plots the maximum surface slope (G) normalized by the critical diameter (w_{cri}) as a function of the overburden friction angles ( ) for various deformation moduli (E_m). For each deformation modulus, the normalized maximum slope (G/w_{cri}) increases with the friction angle, which can be represented by an exponential equation. Their empirical constants A_0 and B_0 depend on the deformation modulus. A power equation can be used to correlate A_0 and B_0 with the deformation modulus E_m, as shown in Figure 7. The normalized maximum slope can be expressed as:

$$G/w_{cri} = 0.0012E_m^{-0.849} \exp(0.0103\phi E_m^{0.27}) \quad (5)$$

The cavern depth at the critical condition decreases with increasing deformation modulus (Figure 8). The depth normalized by the critical diameter (d/w_{cri}), can be expressed as a function of E_m as:

$$d/w_{cri} = (-0.0213\phi^{-0.636})E_m + 1.55\exp(-0.0163\phi) \quad (6)$$

Similar to the derivation above, the relationships for the vertical deformation of the cavern roof (R_S) and the radius of influence on the surface (B/2) can also be developed (Figures 9 and 10).

$$R_s/S_{max,cri} = (10^{-5}\phi - 0.0058)E_m - 0.0519\phi + 4.393 \quad (7)$$

$$B/w_{cri} = 0.11\exp(-0.058\phi)E_m + 2.844\exp(-0.0094\phi) \quad (8)$$

The same procedure is used for the sub-critical condition. The correlation results are shown in Figures 11 through 13, and can be expressed by the following equations:

$$G/w = 0.0012E_m^{-0.412} \cdot (S_{max}^{0.36E_m^{0.12}}) \quad (9)$$

$$d/w = (-0.0002E_m + 0.132)G^{(-0.7E_m^{-0.1743})} \quad (10)$$

$$R_s/w = (0.205E_m^{-0.701}) \cdot S_{max}^{(0.0432E_m^{0.386})} \quad (11)$$

The computer simulations are compared with those calculated by Singh's hyperbolic function for some cases in Figure 14. FLAC simulation gives the subsidence magnitudes about 10% greater than those from the hyperbolic function. The maximum surface slopes calculated from both methods are similar.

5 EXAMPLE OF CALCULATION

This section shows how to determine the cavern depth and diameter from an example set of survey data, as given in Table 1. Regression of these data using equation (1) results in a maximum subsidence at the center of the cavern equal to 0.46 m. Equation (3) determines the maximum slope at the inflection point as 0.013. This example assumes that the deformation modulus of the overburden is known and equal to 20 MPa, with a friction angle equal to 40°. This example assumes that the groundwater table is at the ground surface.

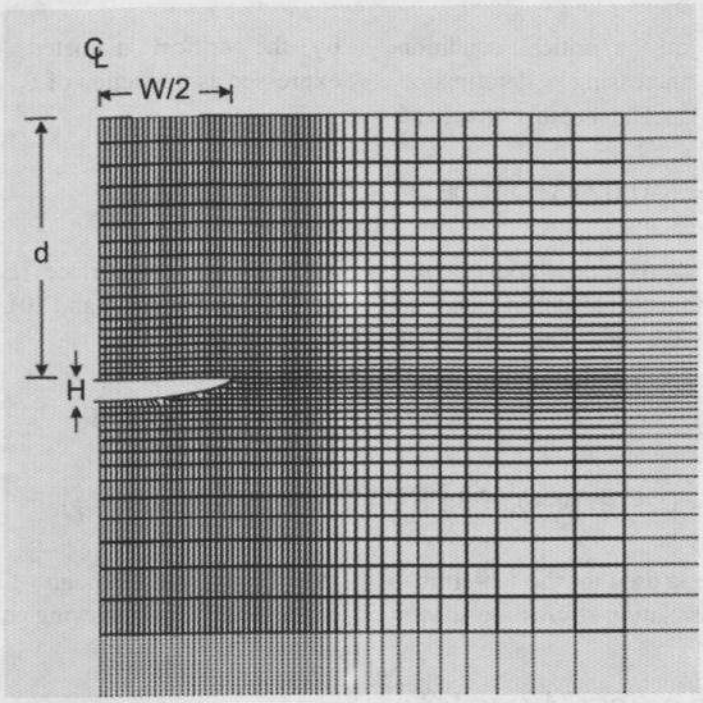

Figure 6. Example of finite difference mesh used in FLAC simulation. Analysis is made in axial symmetry. H = 5 m, d = 60 m, w = 60 m, B = 172 m, E_m = 40 MPa and = 20°.

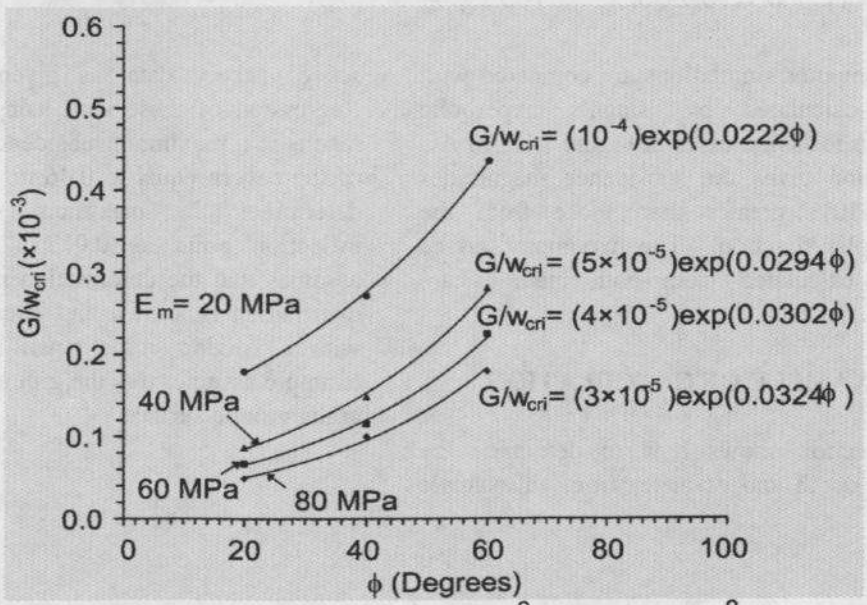

$G/w_{cri} = A_0 \cdot \exp(B_0\phi)$, where; $A_0 = \alpha_{A0} \cdot E_m^{\beta_{A0}}$, $B_0 = \alpha_{B0} \cdot E_m^{\beta_{B0}}$

E_m (MPa)	A_0	α_{A0}	β_{A0}	B_0	α_{B0}	β_{B0}
20	10^{-4}	0.0012	-0.849	0.0222	0.0103	0.27
40	5×10^{-5}			0.0294		
60	4×10^{-5}			0.0302		
80	3×10^{-5}			0.0324		

Figure 7. Maximum slope to critical cavern width ratio (G/w_{cri}) as a function of friction angle ( ) for various deformation moduli (E_m). A_0, B_0, α_{A0}, β_{A0}, α_{B0} and β_{B0} are empirical constants.

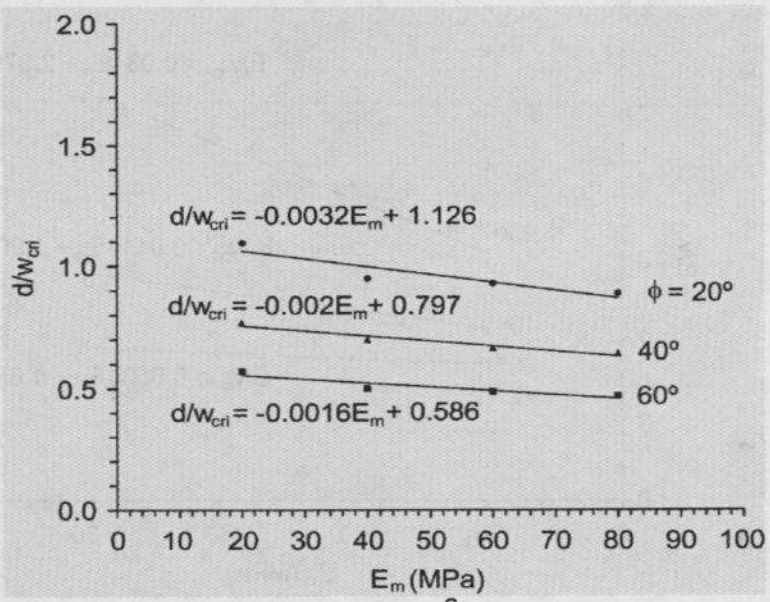

$d/w_{cri} = -A_1 \cdot E_m + B_1$, where; $A_1 = \alpha_{A1} \cdot \phi^{\beta_{A1}}$; $B_1 = \alpha_{B1} \cdot \exp(\beta_{B1} \cdot \phi)$

ϕ (Degrees)	A_1	α_{A1}	β_{A1}	B_1	α_{B1}	β_{B1}
20	0.0032	0.0213	-0.636	1.126	1.55	-0.0163
40	0.0020			0.797		
60	0.0016			0.586		

Figure 8. Cavern depth to critical cavern width ratio (d/w_{cri}) as a function of deformation modulus (E_m) for various friction angles ( ). A_1, B_1, α_{A1}, β_{A1}, α_{B1} and β_{B1} are empirical constants.

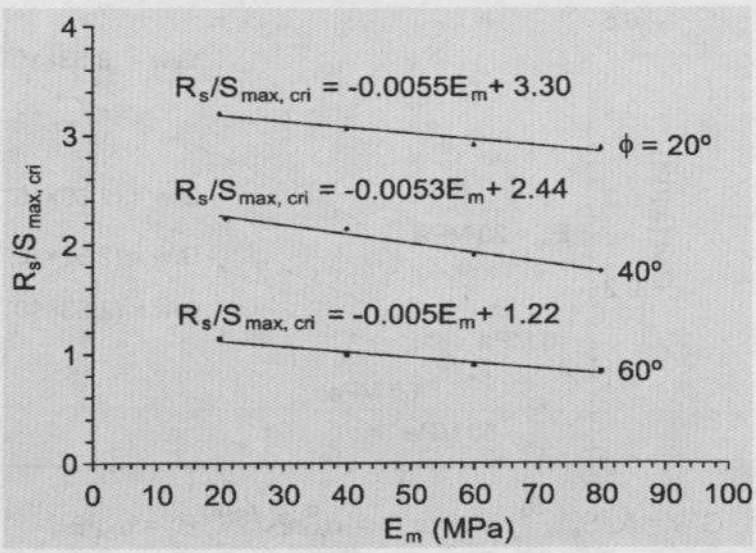

$R_s/S_{max,cri} = -A_2 \cdot E_m + B_2$, where; $A_2 = \alpha_{A2} \cdot \phi + \beta_{A2}$; $B_2 = \alpha_{B2} \cdot \phi + \beta_{B2}$

ϕ (Degrees)	A_2	α_{A2}	β_{A2}	B_2	α_{B2}	β_{B2}
20	0.0055	-10^{-5}	0.0058	3.30	-0.0519	4.393
40	0.0053			2.44		
60	0.0050			1.22		

Figure 9. Roof deformation to maximum subsidence ratio at critical condition ($R_s/S_{max, cri}$) as a function of deformation modulus (E_m) for various friction angles. A_2, B_2, α_{A2}, β_{A2}, α_{B2} and β_{B2} are empirical constants.

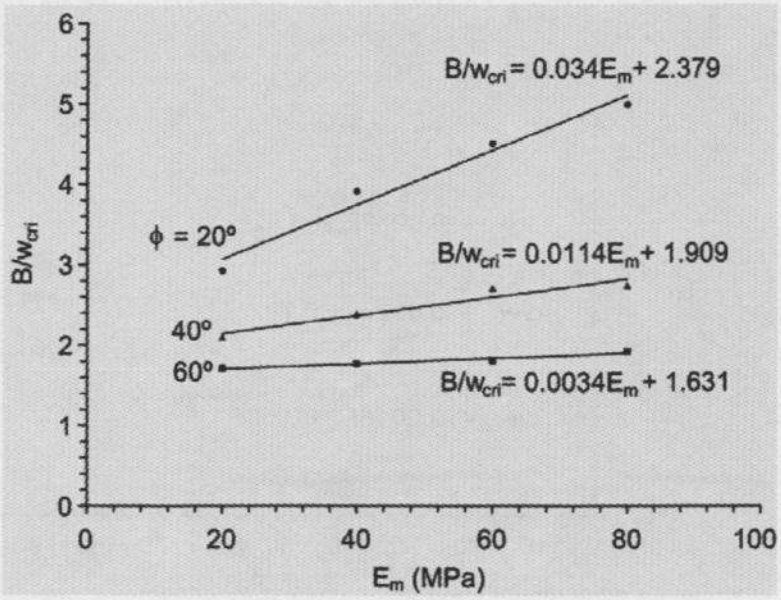

$B/w_{cri} = A_3 \cdot E_m + B_3$, where; $A_3 = \alpha_{A3} \cdot \exp(\beta_{A3} \cdot \phi)$; $B_3 = \alpha_{B3} \cdot \exp(\beta_{B3} \cdot \phi)$

ϕ (Degrees)	A_3	α_{A3}	β_{A3}	B_3	α_{B3}	β_{B3}
20	0.0340	0.11	-0.058	2.379	2.844	-0.0094
40	0.0114			1.909		
60	0.0034			1.631		

Figure 10. Diameter of influence to critical cavern width ratio (B/w_{cri}) as a function of deformation modulus (E_m) for various friction angles. A_3, B_3, α_{A3}, β_{A3}, α_{B3} and β_{B3} are empirical constants.

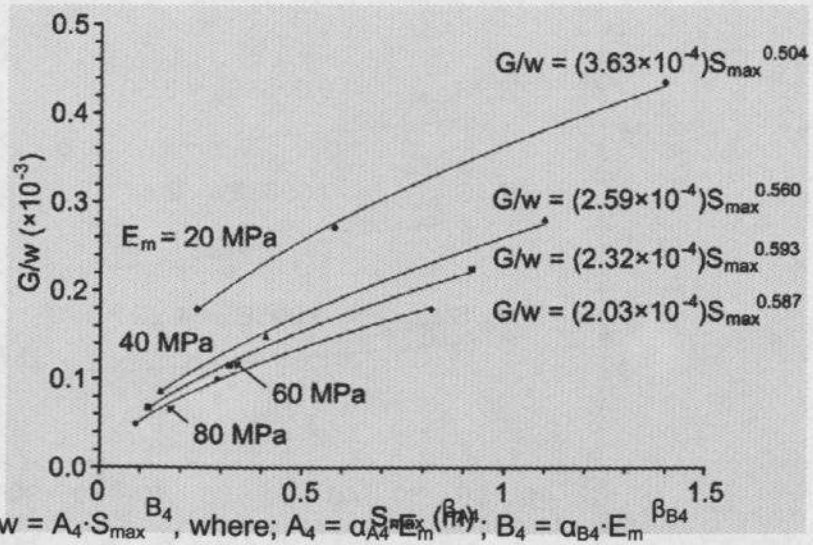

$G/w = A_4 \cdot S_{max}^{B_4}$, where; $A_4 = \alpha_{A4} \cdot E_m^{\beta_{A4}}$; $B_4 = \alpha_{B4} \cdot E_m^{\beta_{B4}}$

E_m (MPa)	A_4	α_{A4}	β_{A4}	B_4	α_{B4}	β_{B4}
20	3.63×10^{-4}	0.0012	-0.412	0.504	0.36	0.12
40	2.59×10^{-4}			0.560		
60	2.32×10^{-4}			0.593		
80	2.03×10^{-4}			0.587		

Figure 11. Maximum slope to cavern width ratio (G/w) as a function of maximum subsidence (S_{max}) for various defromation moduli (E_m). A_4, B_4, α_{A4}, β_{A4}, α_{B4} and β_{B4} are empirical constants.

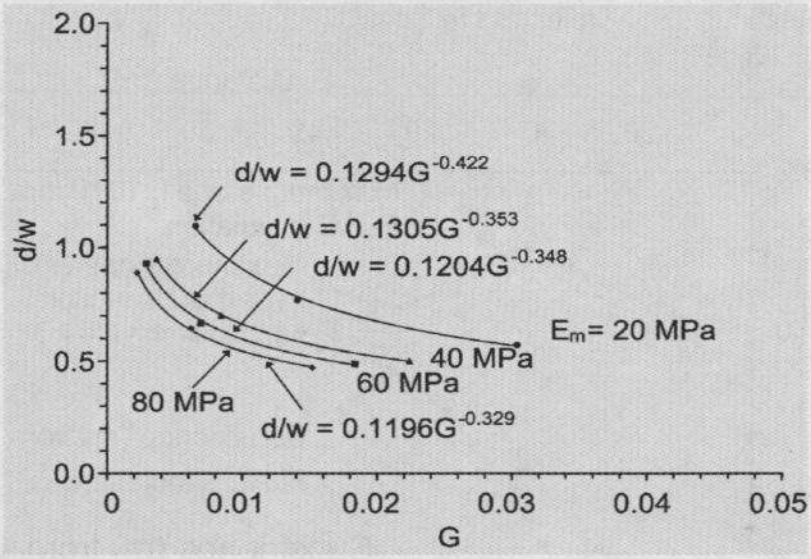

$d/w = A_5 \cdot G^{-B_5}$, where; $A_5 = \alpha_{A5} \cdot E_m + \beta_{A5}$; $B_5 = \alpha_{B5} \cdot E_m^{\beta_{B5}}$

E_m (MPa)	A_5	α_{A5}	β_{A5}	B_5	α_{B5}	β_{B5}
20	0.1294	-0.0002	0.132	0.422	0.7	-1.743
40	0.1305			0.353		
60	0.1204			0.348		
80	0.1196			0.329		

Figure 12. Cavern depth to cavern width ratio (d/w) as a function of maximum slope (G) for various deformation moduli (E_m). A_5, B_5, α_{A5}, β_{A5}, α_{B5} and β_{B5} are empirical constants.

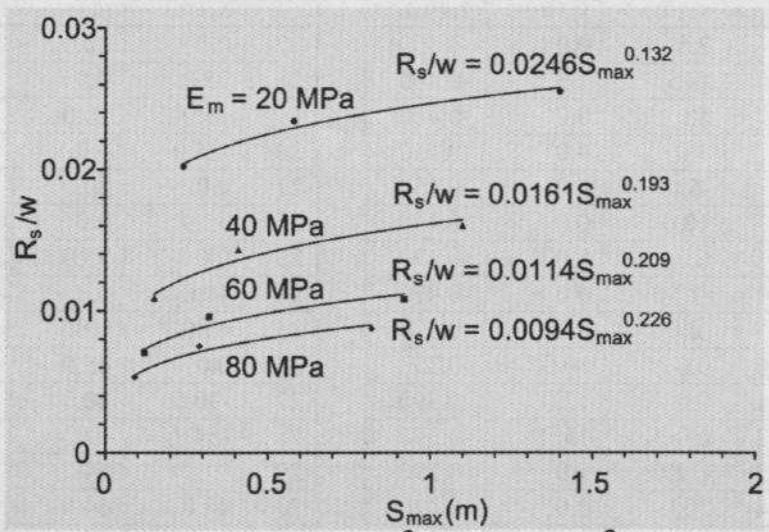

$R_s/w = A_6 \cdot S_{max}^{B_6}$, where; $A_6 = \alpha_{A6} \cdot E_m^{\beta_{A6}}$; $B_6 = \alpha_{B6} \cdot E_m^{\beta_{B6}}$

E_m (MPa)	A_6	α_{A6}	β_{A6}	B_6	α_{B6}	β_{B6}
20	0.0246	0.205	-0.701	0.132	0.0432	0.386
40	0.0161			0.193		
60	0.0114			0.209		
80	0.0094			0.226		

Figure 13. Ratio of roof deformation to cavern width ratio (R_s/w) as a function of maximum subsidence (S_{max}) for various deformation moduli (E_m). A_6, B_6, α_{A6}, β_{A6}, α_{B6} and β_{B6} are empirical constants.

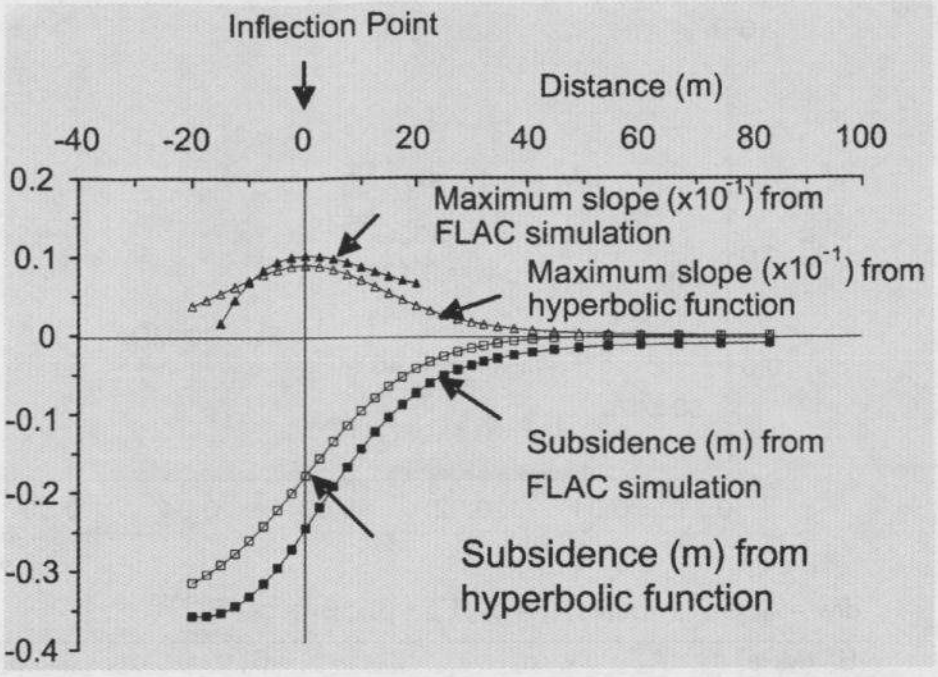

Figure 14. FLAC simulations compared with hyperbolic function calculations for = 20°, E_m = 20 MPa, d = 40 m and w = 40 m.

Table 1. Example of ground survey data measured in subsiding area.

i	x_i (m)	y_i (m)	z_i (m)
1	2.5	0.0	-0.400
2	-2.5	2.5	-0.400
3	5.0	0.0	-0.400
4	3.0	4.0	-0.450
5	-5.0	5.0	-0.450
6	10.0	0.0	-0.450
7	6.0	8.0	-0.470
8	-10.0	0.0	-0.470
9	-6.0	8.0	-0.390
10	0.0	10.0	-0.390
11	9.0	12.0	-0.390
12	0.0	15.0	-0.390
13	-12.0	9.0	-0.390
14	20.0	0.0	-0.420
15	12.0	16.0	-0.420
16	-12.0	16.0	-0.270

i	x_i (m)	y_i (m)	z_i (m)
17	0.0	20.0	-0.270
18	25.0	0.0	-0.270
19	15.0	20.0	-0.270
20	-25.0	0.0	-0.270
21	0.0	30.0	-0.270
22	35.0	0.0	-0.250
23	0.0	35.0	-0.250
24	40.0	0.0	-0.250
25	45.0	0.0	-0.150
26	0.0	45.0	-0.150
27	-30.0	40.0	-0.150
28	-54.7	0.0	-0.050
29	0.0	54.7	-0.050
30	48.0	64.0	-0.015
31	0.0	80.0	-0.015
32	-48.0	64.0	-0.015

Under critical condition the cavern diameter and depth can be estimated from equations (5) through (7), as 54.6 m and 41.9 m. The roof deformation and radius of influence are 1.02 m and 59.2 m. If the ground is under sub-critical condition, the cavern diameter and depth are predicted as 55.6 m and 43.2 m, with the roof deformation and radius of influence equal to 1.25 m and 60.3 m. It can be seen that the solutions are not unique depending on whether the cavern is under sub-critical or critical condition. The cavern diameter, roof deformation and radius of influence can however be calculated if the cavern depth can be pre-defined.

Within the brine pumping areas, the depth of the cavern roof or of the overburden-salt interface can often be determined from interpolating or extrapolating from the existing drill holes or brine pumping wells.

6 SUPER-CRITICAL CONDITION

Two scenarios can occur when the subsidence reaches its super-critical condition, which is dictated by the cavern height. If the cavern height is equal to or less than the roof deformation, the immediate roof rock will touch the cavern floor. Vertical movement of the ground may or may not continue depending on whether the salt floor dissolution is continued. In this case, the subsidence is likely to be small, the subsiding area is relatively flat, and development of a sinkhole is unlikely.

If the cavern height is however significantly greater than the critical roof deformation, failure of the cavern roof can occur under the super-critical condition. The failure can progress upward and may lead to a sinkhole development. In this case, the cavern location can be evidently defined, but accurate prediction of the cavern diameter and depth is virtually impossible. Subsurface investigations by Jenkunawat (2005) and Wannakao & Walsri (2007) reveals that collapsing of the roof rock above some caverns in a brine pumping area has also resulted in a large void remaining in the overburden.

7 DISCRETE ELEMENT ANALYSES

The difficulty in predicting the cavern configurations under super-critical condition is due to the complexity of the post failure behavior of the rock mass and movement of the joint system. To demonstrate these issues, discrete element analyses are performed using UDEC code (Itasca, 2004) to simulate the movement of the jointed rock mass above an isolated salt cavern. The discrete element models are constructed to represent a cavern dissolved at the overburden-salt interface.

The cavern depth, diameter and height are maintained constant at 40 m, 100 m and 30 m, representing a super-critical condition. A hydrostatic stress is applied on both sides of the model. For the first series of simulations there are two mutually perpendicular joint sets inclined at 45°, with friction angles varying from 20°, 30° and 40°. The second series assesses the effect of joint orientation by using a constant joint friction angle of 30°, and varying the joint orientations from 15°, 30° to 45°. The joint spacing for both cases is 8 m.

Simulation results from the first series (shown in Figure 15), suggest that even under the same cavern geometry and joint orientation, different joint friction angles can cause significantly different post-failure conditions. For the overburden with low-friction joints, the cavern can be completely filled with the collapsing rock blocks. This results in a deep sinkhole or a large depression area, or both. Gaps or voids can be formed if the overburden has joints with a higher friction angle, resulting in a shallower sinkhole and smaller subsiding area.

For the second series, Figure 16 compares the simulated results under the same joint friction ($\phi = 30°$) but different joint angles. Different patterns of block collapsing can be obtained for the joints with 30° and 45° inclinations. It is interesting to observe that with the joint angle of 15° the roof failure does not progress upward, and has virtually no impact on the ground surface.

The numerical simulations under the assumed joint conditions above clearly demonstrate the complexity and uncertainty of the subsidence under super-critical condition which can not be easily determined by the analytical method proposed here. Detailed subsurface investigation is required to understand the failure and movement of the overburden under the super-critical condition.

8 CONCLUSIONS

Regression analysis of the ground survey data can provide a smooth and representative profile of the surface subsidence which agrees reasonably well with the hyperbolic function proposed by Singh (1992). An analytical method developed from the results of finite difference analyses can be used to determine the cavern depth and diameter under

sub-critical and critical conditions. Under which condition the cavern belongs to can be defined if the cavern depth is known, in most cases probably by interpolating between nearby boreholes or exploratory wells. The correlations of the subsidence components with the overburden mechanical properties and cavern geometry are applicable to the range of site conditions specifically imposed here (e.g., half oval-shaped cavern created at the overburden-salt interface, horizontal rock units, flat ground surface, and saturated condition). These relations may not be applicable to other subsidence induced under different rock characteristics or different configurations of the caverns. The proposed method is not applicable under super-critical conditions where post-failure behavior of the overburden rock mass is not only unpredictable but also complicated by the system of joints, as demonstrated by the results of the discrete element analyses. The proposed method is useful as a predictive tool to identify the configurations of a solution cavern and the corresponding subsidence components induced by the brine pumping practices. Subsequently, remedial measures can be implemented to minimize the impact from the cavern development before severe subsidence or sinkhole occurs.

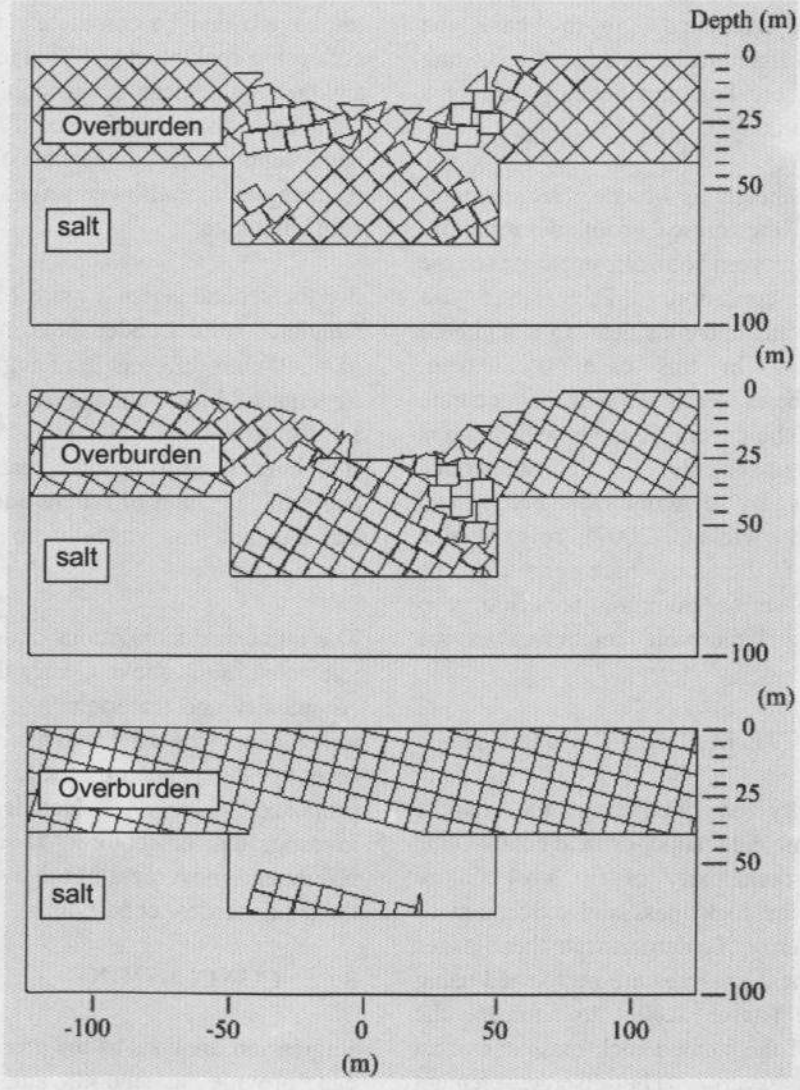

Figure 15. UDEC simulations for cavern roof failure for joints with friction angles of 20° (top), 30° (middle) and 40° (bottom). H = 30 m, d = 40 m, w = 100 m.

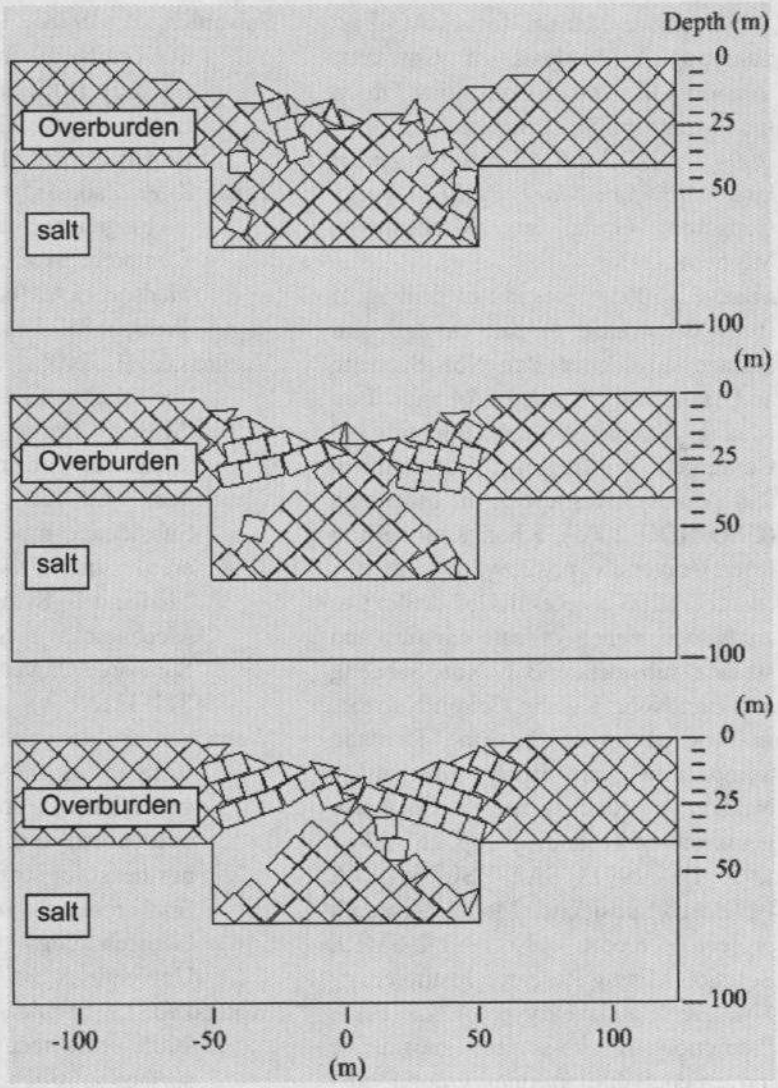

Figure 16. UDEC simulations for cavern roof failure with joint dip angles of 45° (top), 30° (middle) and 15° (bottom). H = 30 m, d = 40 m, w = 100 m.

ACKNOWLEDGEMENT

The research is funded by Suranaree University of Technology. Permission to publish this paper is gratefully acknowledged.

REFERENCES

Asadi, A., Shahriar, K., Goshtasbi, K., & Najm, K., 2005. Development of new mathematical model for prediction of surface subsidence due to inclined coal-seam mining. Journal of the South African Institute of Mining and Metallurgy. 105: 15-20.

Crosby, K., 2007. Integration of rock mechanics and geology when designing the Udon South sylvinite mine. In Proceedings of the First Thailand Symposium on Rock Mechanics, Nakhon Ratchasima: Suranaree University of Technology. pp. 3-22.

Cui, X., Miao, X., Wang, J., Yang, S., Liu, H., Song, Y., Liu, H., & Hu, X., 2000. Improved prediction of differential subsidence caused by underground mining. International Journal of Rock Mechanics and Mining Sciences, Beijing: Pergamon Press, 37(4): 615-627.

Fuenkajorn, K., 2002. Design guideline for salt solution mining in Thailand, Research and Development journal of the Engineering Institute of Thailand, pp. 1-8.

Itasca, 1992. User Manual for FLAC–Fast Langrangian Analysis of Continua, Version 4.0. Itasca Consulting Group Inc., Minneapolis, Minnesota.

Itasca, 2004. *UDEC 4.0 GUI A Graphical User Interface for UDEC*. Itasca Consulting Group Inc., Minneapolis, Minnesota.

Jenkunawat, P., 2005. Results of drilling to study occurrence of salt cavities and surface subsidence Ban Non Sabaeng and Ban Nong Kwang, Amphoe Ban Muang, Sakon Nakhon. International Conference on Geology, Geotechnical and Mineral Resources of Indochina (GEOINDO 2005), Khon Kaen: Khon Kaen University. pp. 259-267.

Jenkunawat, P., 2007. Results of drilling to study occurrence of salt cavities and surface subsidence Ban Non Sabaeng and Ban Nong Kwang, Sakon Nakhon. In Proceedings of the First Thailand Symposium on Rock Mechanics, Nakhon Ratchasima: Suranaree University of Technology. pp. 257-274.

Nieland, J. D. (1991) SALT_SUBSID: A PC-Based Subsidence Model, Research project report No.1991-2-SMRI, Solution Mining Research Institute.

Shu, D.M., & Bhattacharyya, A.K., 1993. Prediction of sub-surface subsidence movements due to underground coal mining. Geotechnical and Geological Engineering. Springer Netherlands. 11(4): 221-234.

Singh, M. M., 1992. Mine subsidence. SME Mining Engineering Handbook. Hartman, H.L. (ed). Society for mining metallurgy and exploration, Inc., Littleton: Colorado. pp. 938-971.

Suwanich, P., 1978. Potash in northeastern of Thailand (in Thai). Economic Geology Document No. 22. Bangkok: Economic Geology, Division, Department of Mineral Resources.

Thiel, K & Zabuski, L., 1993. Rock mass investigations in hydroengineering. Comprehensive Rock Engineering. Hudson, J.A. (ed). London: Pergamon Press, 3: 839-861.

Vattanasak, H., 2006. Salt reserve estimation for solution mining in the Khorat basin, M.Eng. Thesis, Nakhon Ratchasima: Suranaree University of Technology.

Wannakao, L. & Walsri, C., 2007. Subsidence models in salt production area. In Proceedings of the First Thailand Symposium on Rock Mechanics, Nakhon Ratchasima: Suranaree University of Technology. pp. 311-321.

Wannakao, L., Janyakorn, S., Munjai, D., & Vorarat, A., 2004. Geological and geotechnical properties analysis of overburden and salt formations in the northeast for surface subsidence model, final research report, Department of Geotechnology, Khon Kaen University. (in Thai)

Wannakao, L., Munjai, D., & Janyakorn, S., 2005. Geotechnical investigation of surface subsidence at Ban Non Sabaeng salt production area, Sakon Nakhon, Thailand. International Conference on Geology, Geotechnical and Mineral Resources of Indochina (GEOINDO 2005). Khon Kaen: Khon Kaen University. pp. 282.

Warren, J., 1999. Evaporites: Their Evolution and Economics, Oxford: Blackwell Science.